Probing the Limits of Conventional Extended X-ray Absorption Fine Structure Analysis Using Thiolated Gold Nanoparticles

Samuel T. Chill,[†] Rachel M. Anderson,[‡] David F. Yancey,[‡] Anatoly I. Frenkel,[§] Richard M. Crooks,[‡] and Graeme Henkelman*[,†]

[†]Department of Chemistry and the Institute for Computational Engineering and Sciences and [‡]Department of Chemistry, The University of Texas at Austin, Austin, Texas 78712-0165, United States and [§]Physics Department, Yeshiva University, 245 Lexington Avenue, New York, New York 10016, United States

ABSTRACT We present a method for quantifying the accuracy of extended X-ray absorption fine structure (EXAFS) fitting models. As a test system, we consider the structure of bare Au_{147} nanoparticles as well as particles bound with thiol ligands, which are used to systematically vary disorder in the atomic structure of the nanoparticles. The accuracy of the fitting model is determined by comparing two distributions of bond lengths: (1) a direct average over a molecular dynamics (MD) trajectory using forces and energies from density functional theory (DFT) and (2) a fit to the theoretical EXAFS spectra generated from that same trajectory. Both harmonic and quasi-harmonic EXAFS fitting models are used to characterize the first-shell Au—Au bond length distribution. The harmonic model is found to significantly underestimate the coordination number, disorder, and bond length. The quasi-harmonic model, which includes the third cumulant of the first-shell bond length distribution, yields accurate bond lengths, but incorrectly predicts a decrease in particle size and little change in the disorder with increasing thiol ligands. A direct analysis of the MD data shows that the particle surfaces become much more disordered with ligand binding, and the high disorder is incorrectly interpreted by the EXAFS fitting models. Our DFT calculations compare well with experimental EXAFS measurements of Au nanoparticles, synthesized using a dendrimer encapsulation technique, showing that systematic errors in EXAFS fitting models apply to nanoparticles 1—2 nm in size. Finally we show that a combination of experimental EXAFS analysis with candidate models from DFT is a promising strategy for a more accurate determination of nanoparticle structures.

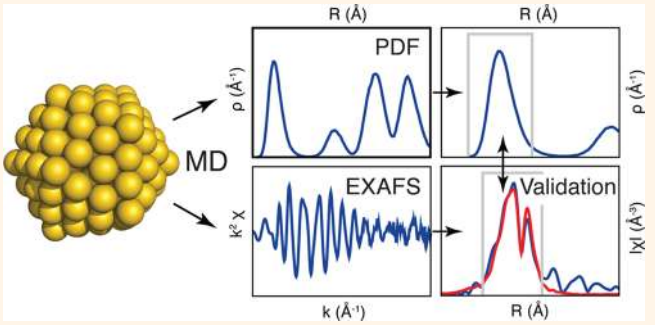

KEYWORDS: extended X-ray absorption fine structure · density functional theory · Au nanoparticles · structural disorder

Extended X-ray absorption fine structure (EXAFS) spectroscopy is a powerful tool for determining local atomic structure. *In situ* EXAFS analysis is particularly useful for studying catalysts because changes in the local atomic structure at the surface of a catalyst under reaction conditions can dramatically change the catalytic activity.[1,2] While EXAFS is not surface-sensitive, catalytic particles on the scale of 1—2 nm have a similar number of surface as bulk atoms, so that surface structure contributes significantly to the total signal.

Nanoparticles in the sub-2 nm size range can have significantly different properties from the bulk material. While the surfaces of larger particles can be modeled as bulk slabs, the surface chemical properties of particles in the size range considered here depend on their full 3D structure.[3] This makes the experimental determination of a unique 3D structure a high priority goal in understanding their chemical behavior. Recently some advancements have been made in reconstructing a 3D electron density map from electron microscopy experiments to solve for the structure of Au nanoparticles.[4] However, EXAFS remains a widely used tool for structural characterization due to its elemental specificity and that ensemble averages may be obtained. As EXAFS reveals only local structural information, recent studies have demonstrated the merits of combined EXAFS and *ab initio* theoretical calculations

* Address correspondence to henkelman@utexas.edu.

Received for review January 6, 2015 and accepted April 8, 2015.

Published online April 08, 2015
10.1021/acsnano.5b00090

to obtain a more detailed understanding of the structure.[5,6]

The analysis of EXAFS is well-established for bulk materials in which the local atomic structure is repeated throughout the material. There is more uncertainty about the appropriate use and accuracy of EXAFS fitting models to determine the structure of nanoparticles. The challenge associated with nanoparticles is that they have greater disorder in structure as compared to bulk, which is correlated to the position in the particle (*e.g.*, a contraction of bonds at the surface of the particle).[7] The interference pattern in an EXAFS measurement emphasizes the ordered component of the structure over the disordered components.[8] As we will show here, disorder can also be convoluted with other fitting parameters, giving rise to systematic errors in the fit values of interatomic distances in the particle or the average coordination number of the atoms in the particle. The quantification of such systematic errors in determining nanoparticle structure as a result of the EXAFS fitting model is the focus of this paper.

Key to our study of EXAFS fitting models is a computational technique designed to test the self-consistency of the EXAFS analysis, as illustrated in Figure 1. Candidate nanoparticle structures are generated and modeled using density functional theory (DFT). Molecular dynamics (MD) trajectories give an ensemble average of structures, from which pair-correlation data between the atoms are collected. Analysis of the pair distribution function (PDF) generated from the MD trajectory allows for a direct calculation of the average number of neighbors N, the average bond length R, and a measure of the disorder in the bond length distribution σ^2, quantified by the Debye–Waller factor. We take this PDF data and the structural parameters derived directly from it as the target for EXAFS analysis. We then simulate the EXAFS spectrum by averaging the scattering over each structure in the ensemble and use the same EXAFS equations to model the spectrum and determine best-fit values of N, R, and σ^2. Comparison with the corresponding values from the structural models used to generate the EXAFS spectra gives us a measure of how appropriate the fitting model is and a quantification of any systematic errors present.

Importantly, this approach does not rely on an accurate simulation of EXAFS spectra as compared to what is observed in an experiment. It is still valuable, however, to connect with experiment in order to understand if systematic errors in EXAFS fits are being made in the determination of real nanoparticle structures. Accordingly, we compare our theory to experimental EXAFS measurements of Au nanoparticles and show that a standard EXAFS fit using a bulk reference model with a normal distribution of first-neighbor bonds gives rise to significant errors in the fitted parameters. The systematic error is shown to increase with disorder, induced by the binding of thiol groups to the nanoparticle surface.

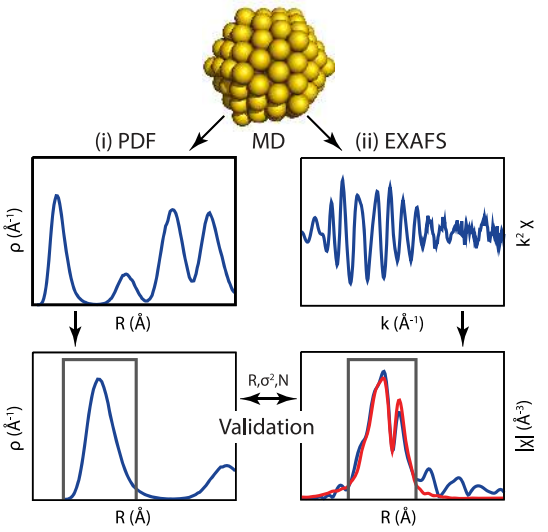

Figure 1. Scheme for testing the self-consistency of an EXAFS model: (i) a dynamical trajectory of, in this case, a nanoparticle is simulated and the pair distribution function (PDF) of bond lengths is collected, and (ii) the EXAFS spectrum is modeled as an average over the trajectory and subsequently fit using the same EXAFS equations. The resulting parameters, including the average bond length R, number of neighbors N, and the Debye–Waller factor σ^2, are compared to the direct MD simulation.

A quasi-harmonic fitting model using the cumulant expansion method is also considered, to include anharmonic corrections to the PDF. Anharmonicity can account for the non-Gaussian disorder (both static and dynamic) that arises in nanoparticle systems and offers a significant improvement over the Gaussian model in predicting mean bond lengths.

Finally, we suggest that DFT modeling can be used in concert with experimental EXAFS measurements to improve the determination of nanoparticle structures. Since EXAFS does not provide a unique structure, DFT can help to evaluate the relative weight of candidate structures based upon the calculated total energy. Additionally, explicit theoretical modeling of the EXAFS spectra from many candidate structures and a subsequent comparison to experiment can be used to determine structures that are consistent with the experimental data, without relying on a fitting model.

EXAFS Modeling. EXAFS spectra provide information about local atomic structure around the X-ray absorbing atoms. The functional form of the spectrum contains many terms, but can be roughly described as exponentially decaying sinusoids, whose amplitudes, frequencies, and decay rates are correlated with coordination numbers, bond lengths, and structural disorder, respectively. A model for EXAFS describes the single scattering between the adsorbing atom and neighboring atoms at a distance r_i:

$$\chi(k) = \sum_i \frac{N_i S_0^2 F_i(k)}{k} \int_0^\infty g(r_i) \frac{\exp(-2r_i/\lambda_i(k))}{r_i^2} \times \sin(2kr_i + \delta_i(k))\, dr_i \quad (1)$$

Here i is a path index that represents different types of scattering paths (*e.g.*, Au−Au or Au−S); $g(r_i)$ is the probability density of finding a neighbor atom at r_i; N_i is the average coordination number; k is the photoelectron wavenumber; S_0^2 is the amplitude reduction factor; $\lambda_i(k)$ is the mean free path of the photoelectron; $F_i(k)$ is the effective scattering amplitude; and $\delta_i(k)$ is the effective phase shift. For an in-depth explanation of EXAFS and related techniques see ref 9.

Theoretical standards can be used to determine the effective scattering amplitude $F_i(k)$, the phase shift $\delta_i(k)$, and the photoelectron mean free path $\lambda_i(k)$.[10] The amplitude reduction factor S_0^2 and the correction to the energy origin ΔE_0 can be determined by fits to experimental standards (*e.g.*, a metal foil) and also recently by the use of theoretical standards.[10] This leaves $g(r_i)$ as the only unknown in eq 1.

To extract structural information from $g(r_i)$, a fitting model must be assumed. The use of the cumulant expansion method allows for eq 1 to be expanded in a series.[11] By truncating the series to the first two terms, a harmonic model for the bond length distribution is obtained. This model is appropriate for systems with a low to moderate level of disorder. The resulting EXAFS equation is

$$\chi_2(k) = \sum_i \frac{N_i S_0^2 F_i(k)}{kR_i^2} \exp(-2R_i/\lambda_i(k)) \times \exp(-2k^2\sigma_i^2)\sin(2kR_i + \delta_i(k)) \quad (2)$$

The bond length distribution is now described by a Gaussian-shaped distribution centered at R_i with a variance of σ_i^2. The variance is often referred to as the Debye−Waller factor (DWF).

In systems with a high level of disorder the harmonic model is insufficient and a higher order cumulant expansion should be used. A quasi-harmonic model introduces the third cumulant of the distribution, C_3, which is a measure of how skewed the bond length distribution is from a symmetric Gaussian distribution.

$$\chi_3(k) = \sum_i \frac{N_i S_0^2 F_i(k)}{kR_i^2} \exp(-2R_i/\lambda_i(k)) \times \exp(-2k^2\sigma_i^2)\sin\left(2kR_i - \frac{4k^3}{3}C_3 + \delta_i(k)\right) \quad (3)$$

A more detailed derivation of the cumulant expansion method can be found in ref 11.

RESULTS

$Au_{147}@S_n$ nanoparticles were synthesized with a dendrimer template technique and characterized using EXAFS as described in the Experimental Details section. The EXAFS spectrum of Au_{147} nanoparticles is shown in Figure 2a. Within the radial window of the first-neighbor shell, there is remarkable agreement between

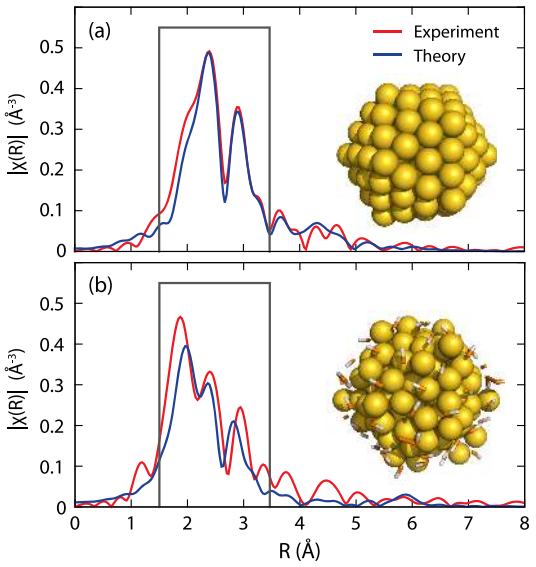

Figure 2. Comparison between theoretically simulated and experimentally measured EXAFS spectra of bare Au_{147} and $Au_{147}@S_{72}$ with 72 thiol ligands bound to the nanoparticle surface.

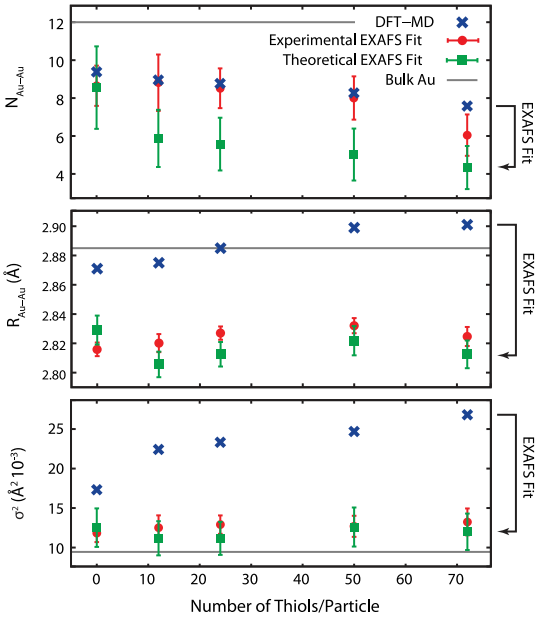

Figure 3. DFT-MD and harmonic EXAFS fit parameters characterizing the first-neighbor shell of Au in Au_{147} and $Au_{147}@S_n$.

experiment and theory, given that there is no fitting involved. The bare Au_{147} particles have modestly more disorder as compared to bulk Au. To consider greater disorder, thiol ligands were bound to the surface.[12,13] Figure 2b shows EXAFS spectra from our DFT-MD model (inset) and experiment. Both of these spectra can be fit using the harmonic model. The resulting fits look quite good (for example, see Figure 3), and the parameters derived from the experimental and theoretical EXAFS spectra simulated from the DFT-MD data are reasonably consistent. The specific values of the coordination

TABLE 1. Fitted Parameters to EXAFS Spectra

system	N	R (Å)	σ^2 (10^{-3} Å^2)	C_3 (10^{-4} Å^3)
Au_{147} experiment[a]	8.7 ± 1.1	2.816(5)	11.8 ± 1.1	
Au_{147} theory[a]	8.6 ± 2.2	2.829(10)	12.5 ± 2.4	
Au_{147} experiment[b]	9.0 ± 1.0	2.838(10)	12.0 ± 1.0	5.3 ± 2.1
Au_{147} theory[b]	8.8 ± 0.9	2.859(9)	12.5 ± 1.0	7.3 ± 2.1
Au_{147} DFT-MD	**9.38**	**2.871**	**17.3**	**11.8**
$Au_{147}@S_{72}$ experiment[a]	6.0 ± 1.1	2.825(6)	13.2 ± 1.7	
$Au_{147}@S_{72}$ theory[a]	4.3 ± 1.1	2.812(9)	12.0 ± 2.3	
$Au_{147}@S_{72}$ experiment[b]	6.0 ± 1.0	2.811(14)	13.2 ± 1.5	−3.5 ± 3.1
$Au_{147}@S_{72}$ theory[b]	5.3 ± 0.6	2.878(8)	12.4 ± 0.8	13.5 ± 1.9
$Au_{147}@S_{72}$ DFT-MD	**7.58**	**2.901**	**26.8**	**20.8**

[a] Using harmonic model. [b] Using quasi-harmonic model.

number N, the bond length R, and Debye−Waller factor σ^2 are reported in Table 1.

The agreement between the experimental and theoretical EXAFS fitting values is better for the bare Au_{147} particles than for the $Au_{147}@S_{72}$ particles. This is because the simulated Au_{147} spectrum is a better match to the experiment (see Figure 2). It is not surprising that the spectrum of the highly disordered $Au_{147}@S_{72}$ system is more challenging to reproduce. In our DFT-MD simulations, only a single $Au_{147}@S_{72}$ particle is modeled for 10 ps, while in the EXAFS experiment an ensemble of particles is observed over an experimental time scale of minutes.

While there is reasonable agreement between the experimental EXAFS spectra and the one based upon our DFT model, this is not enough to say that the model is correct. In fact there is a wide range of structural models that are consistent with a nanoparticle EXAFS spectrum. Furthermore, we will argue next that standard (harmonic and quasi-harmonic) EXAFS fitting models can have an inherent and imperceptible bias toward the model that is used for the fit of disordered nanoparticles.

We can quantify bias in the EXAFS fit using the self-consistent analysis presented in Figure 1. First, the DFT-MD trajectories are analyzed in terms of their first-neighbor distributions to extract average values of N, R, and σ^2. These values are the reference that a subsequent EXAFS analysis should reproduce. Second, the EXAFS spectrum is calculated from the DFT-MD trajectory, and this spectrum is fit using a Gaussian model to give values of N, R, and σ^2, which are compared to the DFT-MD reference values.

Figure 3 shows the EXAFS harmonic fit parameters in comparison to those obtained by direct MD-DFT. The DFT-MD trajectory shows significantly larger values of N, R, and σ^2 as compared to those based upon a fit to the EXAFS spectra generated from the same trajectory data. The standard EXAFS analysis incorrectly indicates that the particles are smaller and more ordered than they really are. Also, the fit parameters from the DFT-MD-simulated EXAFS are much closer to those seen

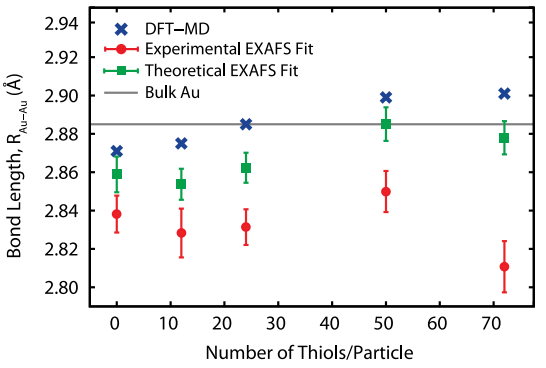

Figure 4. DFT-MD and quasi-harmonic EXAFS mean bond lengths in the first-neighbor shell of Au in Au_{147} and $Au_{147}@S_n$.

in experiment, as compared to those taken directly from the DFT-MD data. This indicates that a harmonic fit to the experimental EXAFS data of these nanoparticle can give structural parameters that are unknowingly many standard deviations away from the actual values.

In order to account for the large static disorder present in the nanoparticle system, the quasi-harmonic fitting model for the Au−Au first shell was also considered. Table 1 compares N, R, σ^2, and C_3 for the theoretical and experimental Au_{147} and $Au_{147}@S_{72}$ particles. The reference DFT-MD values show that there is significant skew toward longer bond lengths (positive C_3) in the bare Au_{147} particle and an even larger skew for $Au_{147}@S_{72}$. The primary improvement provided by this additional degree of freedom in the fitting model is in the bond length. Figure 4 shows that values obtained from the theoretical EXAFS data are accurate and have the correct trend of increasing bond lengths as thiol ligands are bound to the particle.

It is relevant to point out that the theoretical fit has an advantage over the experimental fit in regards to determining the bond length. In the theoretical fit, the correction to the energy origin is exact, since it was fixed to the value used to generate the EXAFS spectra. When ΔE_0 was allowed to float in the fit, it was determined to be 4 eV below the known value, and the mean bond length was significantly underestimated, since ΔE_0 and bond length are correlated parameters in the model. To be consistent, the experimental fit was also given a fixed energy origin, although the effect of having it float was insignificant. Uncertainty in ΔE_0 may explain the differences between the experimental and theoretical bond lengths.

While the bond lengths improve significantly with the use of the quasi-harmonic model, the values of σ^2 and N did not improve across the data set. Consequently, if only EXAFS fitting data were used to analyze the $Au_{147}@S_n$ series, one would reach the qualitatively incorrect conclusion that addition of thiol does not increase the disorder in the particle and instead decreases the Au−Au coordination number and therefore the particle size. The DFT-MD data, however, show

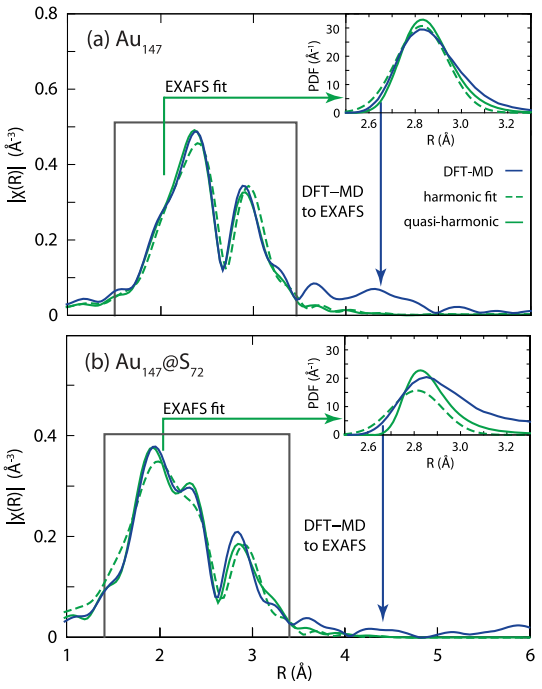

Figure 5. Fits to the theoretical *R*-space EXAFS as well as the resulting bond length distributions are compared to the results from DFT-MD.

a 55% increase in disorder from Au_{147} to $Au_{147}@S_{72}$ and a small decrease in coordination number due only to extreme lengthening of the Au−Au bonds beyond the 3.3 Å first-neighbor cutoff distance.

The range of models that are consistent with the same EXAFS data is illustrated by comparing the first-neighbor bond length distribution from DFT-MD and from the parameters fit to the simulated EXAFS spectra based upon the same DFT-MD data. Figure 5 shows this comparison for Au_{147} and $Au_{147}@S_{72}$. The contrasting fit parameters from Figure 3 are reflected in the distributions, with the Gaussian EXAFS analysis missing the fat tails' long bond lengths seen in the DFT-MD simulations and instead giving a more ordered, narrow distribution with a shorter average bond length.

Since there exists no unique choice for the functional form of the PDF given three cumulants of the distribution (as opposed to the Gaussian form when only two are known), we chose to model the PDF using a Morse potential parametrized to reproduce the average, variance, and skew obtained from the fits. Visualized in this way, the quasi-harmonic fitting model gives rise to distributions that more closely resemble the original DFT-MD distribution, especially for the Au_{147} particles. However, the model does not come close to modeling the level of disorder present in the $Au_{147}@S_{72}$ particles.

DISCUSSION

In this section, we will show how the Gaussian fitting model fails in highly disordered systems. The most important result will be that the fitting model, in this high-disorder regime, interprets an increase in disorder as a reduction in the coordination number and bond length.

To better understand the source of errors in our EXAFS fits, we have constructed model PDFs, based upon a Morse potential, that reproduce the coordination number, mean bond length, DWF, and third cumulant of the DFT-PDF $Au_{147}@S_{12}$ particles. $Au_{147}@S_{12}$ was chosen because these particles have moderate disorder so that the EXFAS fits are reasonably accurate based upon the harmonic model, but the errors are still large enough to be determined. The quantification is done, as previously, by comparing the values of N, R, and σ^2 from the PDF and from the EXAFS fit. We then consider the sensitivity of the fit values with respect to changes in the PDF. Formally, this is a Jacobian matrix relating derivatives of the fit values with respect to the actual changes in the PDF:

$$J = \begin{pmatrix} \frac{\partial N_{fit}}{\partial N} & \frac{\partial N_{fit}}{\partial R} & \frac{\partial N_{fit}}{\partial \sigma^2} \\ \frac{\partial R_{fit}}{\partial N} & \frac{\partial R_{fit}}{\partial R} & \frac{\partial R_{fit}}{\partial \sigma^2} \\ \frac{\partial \sigma^2_{fit}}{\partial N} & \frac{\partial \sigma^2_{fit}}{\partial R} & \frac{\partial \sigma^2_{fit}}{\partial \sigma^2} \end{pmatrix} \quad (4)$$

Ideally J would be the identity matrix indicating that the variables in the EXAFS fitting model are independent. In reality, this is not the case, and the values of the off-diagonal components give a measure of correlation between the parameters, and the values of the on-diagonal elements reflect the sensitivity of the fitted parameter with respect to changes in the PDF. The Jacobian also allows for an analysis of what errors are expected to arise if the PDF is varied, for example by adding disorder due to thiol ligands.

The Jacobian for the EXAFS harmonic model of $Au_{147}@S_{12}$ was evaluated by finite difference as

$$J_{Au_{147}@S_{12}} = \begin{pmatrix} 0.665 & -0.163 & -0.097 \\ 0.000 & 0.687 & -0.281 \\ 0.000 & -0.529 & 0.642 \end{pmatrix} \quad (5)$$

where the rows are the derivatives of the fit values of N, R, and σ^2. Note that R and σ^2 are taken in units of 10^{-2} Å and 10^{-3} Å^2, respectively. This normalization allows for a reasonable comparison of the relative magnitude of the diagonal and off-diagonal values in J, which would otherwise have different units. Interestingly, there are significant off-diagonal terms and all of the diagonal terms are less than 1.

The first column of $J_{Au_{147}@S_{12}}$ indicates that an increase in the amplitude (coordination number) of the PDF will only increase N_{fit}, although only by 70% of what it should. The second column shows more serious problems, specifically that an increase in R will show up as a reduced N and σ^2 in the fit. Most relevant for our study is the third column, which shows that an increased disorder in the actual bond length distribution will be interpreted as a reduction in coordination

number and bond length in the EXAFS fit. Additionally since all of the diagonal elements are less than unity, any actual increase in coordination number, bond length, or disorder will be attenuated in the EXAFS fit.

We can use $J_{Au_{147}@S_{12}}$ to explain the problems in the EXAFS fit for more disordered particles. This will be shown by using the Jacobian for linear expansion of the fit values about $Au_{147}@S_{12}$. The DFT-PDF parameters for $Au_{147}@S_{12}$ and $Au_{147}@S_{72}$ are represented as column vectors:

$$P_{Au_{147}@S_{12}} = (9.0, 2.875\ \text{Å}, 22 \times 10^{-3}\ \text{Å}^2) \quad (6)$$

$$P_{Au_{147}@S_{72}} = (7.6, 2.901\ \text{Å}, 27 \times 10^{-3}\ \text{Å}^2) \quad (7)$$

These values show how the coordination number decreases, bond length increases, and disorder increases from $Au_{147}@S_{12}$ to $Au_{147}@S_{72}$. The values from the harmonic EXAFS fit to $Au_{147}@S_{12}$ are represented in the same way:

$$F_{Au_{147}@S_{12}} = (5.9, 2.806\ \text{Å}, 11 \times 10^{-3}\ \text{Å}^2) \quad (8)$$

Then, the linear expansion makes a prediction for $F_{Au_{147}@S_{72}}$:

$$F_{Au_{147}@S_{72}} \approx F_{Au_{147}@S_{12}} + J_{Au_{147}@S_{12}}(P_{Au_{147}@S_{72}} - P_{Au_{147}@S_{12}}) \quad (9)$$

$$\approx (4.0, 2.810\ \text{Å}, 13 \times 10^{-3}\ \text{Å}^2) \quad (10)$$

The actual fit values, reproduced from Table 1, are (4.3, 2.812 Å, 13×10^{-3} Å^2). So this linear extrapolation correctly indicates that the harmonic EXAFS model will underestimate the coordination number, bond length, and disorder as compared to the underlying PDF of the $Au_{147}@S_{72}$ particles.

CONCLUSIONS

In conclusion, we have presented a self-consistent method for measuring the error in EXAFS fitting models and applied it to the study of disordered $Au_{147}@S_n$ nanoparticles. We show, through the use of DFT-MD simulations, that EXAFS fitting models can significantly underestimate coordination number, bond length, and disorder. Since the simulated EXAFS compares well with that of experimental $Au_{147}@S_n$ dendrimer-encapsulated nanoparticles (DENs), it is consistent that 1−2 nm metal nanoparticles actually have this high level of disorder. Thus, the harmonic and quasi-harmonic cumulant fitting models should be used with caution when fitting nanoparticle data. Trends in disorder and coordination number, for example, should be carefully compared with other sources of data such as DFT simulations in order to interpret the results of the EXAFS fit.

METHODS

Experimental Details. Au_{147} dendrimer-encapsulated nanoparticles were synthesized as previous described[14,15] using sixth-generation amine-terminated (G6-NH_2) poly(amidoamine) dendrimers at a concentration of 2.0 μM. The Au_{147} DENs were modified with differing amounts of 2-mercaptoethanol (2ME). The resulting samples are referred to as $Au_{147}@S_n$, where n is the ratio of 2ME:Au_{147} DENs. In this study, values of n = 0, 12, 24, 50, and 72 were investigated.

Scanning transmission electron microscopy (STEM) micrographs of Au_{147} and $Au_{147}@S_{72}$ were obtained, after the EXAFS analysis, using a JEOL ARM 200F aberration-corrected STEM in order to determine the particle size distribution. Both the Au_{147} and $Au_{147}@S_{72}$ DENs were found to be nearly monodisperse with a size distribution of 1.7 ± 0.3 nm and 1.6 ± 0.3 nm, respectively.

The $Au_{147}@S_n$ solutions were frozen in liquid N_2 and freeze-dried. For EXAFS analysis, the dried $Au_{147}@S_n$ DENs were mixed with a BN binder and pressed under one metric ton of pressure to form a pellet. EXAFS experiments were carried out at the National Synchrotron Light Source (Brookhaven National Laboratory) at beamline X18B. Au L3-edge data were collected at 25 °C in transmission mode using gas ionization detector chambers. Au foil data were collected simultaneously with the sample data in reference mode.

EXAFS Fitting Details. The harmonic and quasi-harmonic fitting models described in eqs 2 and 3 were used to determine N, R, σ^2, and C_3 (in the quasi-harmonic model) for the first-shell Au−Au PDF of nanoparticle gold, from both experimental and theoretical EXAFS data. A fitting model arising from a higher order expansion of the EXAFS equation that includes a fourth cumulant term C_4 was not used because the model gave a lower quality fit, as determined by an increase in the reduced χ^2 statistic. For gold nanoparticles with thiol ligands bound to the surface, the Au−S PDF was modeled as harmonic.

The effective scattering amplitudes, $F_i(k)$, and effective phase shifts, $\delta_i(k)$, were calculated using FEFF6. The amplitude reduction factor S_0^2 and the correction to the energy origin ΔE_0 were determined by a fit to the experimental Au foil.

All nanoparticle fits were performed simultaneously, with the Au−S bond length and Au−S DWF constrained to be the same for each particle, and the ΔE_0 correction to the energy origin was fixed to the experimental bulk foil value. This fitting procedure was carried out using the IFEFFIT software package.[16,17]

Computational Details. DFT was used to simulate the equilibrium structures of the 147-atom Au nanoparticles either bare or with n thiol groups bound to the surface. For each particle, a 10 ps MD simulation was performed at 300 K to obtain representative geometries for structural and EXAFS analysis. We used the Vienna *ab initio* simulation package code[18] with electron correlation treated within the generalized gradient approximation using the PBEsol functional,[19] which is a modified form of Perdew−Burke−Ernzerhof (PBE)[20] with reduced gradient dependence to improve lattice parameters and surface energies in solids. Core electrons were described with the projector augmented-wave method.[21,22] Kohn−Sham wave functions for the valence electrons were expanded in a plane wave basis set with an energy cutoff of 200 eV.

Two possible structures for the Au nanoparticles were investigated: an icosahedron and a cuboctahedron. DFT calculations revealed that the icosahedron was more stable by 3.98 eV. Additionally, DFT-MD simulations of cuboctahedral particles showed spontaneous rearrangement to the icosahedral shape. Due to this evidence, the nanoparticles were modeled as icosahedra. The 2ME molecule was modeled as a (−S−H) ligand to reduce the computational cost as compared to modeling the entire molecule. Nanoparticles were isolated in a cubic box with side lengths of 28 Å to avoid artificial interactions between periodic images.

Theoretical EXAFS signals were simulated using an approach similar to that reported previously.[23] Au L3-edge EXAFS

spectra were calculated from the MD trajectories by averaging the signal arising from each Au atom in the particle. MD trajectories were thermalized for 4 ps, after which the per-configuration EXAFS spectra were calculated from snapshots of the trajectory at intervals of 20 fs for 4 ps, giving 200 independent configurations in the canonical average. Neighboring atoms up to 6 Å away from each photoabsorbing atom were included in the scattering calculations. Once the theoretical EXAFS signal was produced, the correction to the energy origin that was determined from the experimental EXAFS (4.11 eV) was applied to the theoretical data to properly align the experimental and theoretical data in *k*-space.

The Au−Au PDF were produced from similarly sampled snapshots of the DFT-MD trajectories. Theoretical values for Au−Au coordination number, bond length, and bond disorder were calculated from all Au−Au bonding pairs shorter than 3.3 Å, which is the distance where the pair density went to zero for Au_{147}.

Conflict of Interest: The authors declare no competing financial interest.

Acknowledgment. We gratefully acknowledge support from the U.S. Department of Energy under Contract DE-FG02-13ER16428 and the Robert A. Welch Foundation (Grants F-0032 and F-1841). Use of the NSLS is supported by the U.S. Department of Energy, Office of Science, Office of Basic Energy Sciences, under Contract No. DE-AC02-98CH10886. Beamline X18B at the NSLS is supported in part by the Synchrotron Catalysis Consortium, U.S. Department of Energy Grant No. DE-FG02-05ER15688. The computational work was done at the National Energy Research Scientific Computing Center and the Texas Advanced Computing Center.

REFERENCES AND NOTES

1. Tao, F.; Grass, M. E.; Zhang, Y.; Butcher, D. R.; Renzas, J. R.; Liu, Z.; Chung, J. Y.; Mun, B. S.; Salmeron, M.; Somorjai, G. A. Reaction-Driven Restructuring of Rh-Pd and Pt-Pd Core-Shell Nanoparticles. *Science* **2008**, *322*, 932–934.
2. Strasser, P.; Koh, S.; Anniyev, T.; Greeley, J.; More, K.; Yu, C.; Liu, Z.; Kaya, S.; Nordlund, D.; Ogasawara, H.; Toney, M. F.; Nilsson, A. Lattice-Strain Control of the Activity in Dealloyed Core-Shell Fuel Cell Catalysts. *Nat. Chem.* **2010**, *2*, 454–460.
3. Kleis, J.; Greeley, J.; Romero, N.; Morozov, V.; Falsig, H.; Larsen, A.; Lu, J.; Mortensen, J.; Dułak, M.; Thygesen, K.; *et al*. Finite Size Effects in Chemical Bonding: From Small Clusters to Solids. *Catal. Lett.* **2011**, *141*, 1067–1071.
4. Azubel, M.; Koivisto, J.; Malola, S.; Bushnell, D.; Hura, G. L.; Koh, A. L.; Tsunoyama, H.; Tsukuda, T.; Pettersson, M.; Häkkinen, H.; *et al*. Electron Microscopy of Gold Nanoparticles at Atomic Resolution. *Science* **2014**, *345*, 909–912.
5. Behafarid, F.; Matos, J.; Hong, S.; Zhang, L.; Rahman, T. S.; Roldan Cuenya, B. Structural and Electronic Properties of Micellar Au Nanoparticles: Size and Ligand Effects. *ACS Nano* **2014**, *8*, 6671–6681.
6. Rehr, J. J.; Vila, F. D. Dynamic Structural Disorder in Supported Nanoscale Catalysts. *J. Chem. Phys.* **2014**, *140*, 134701.
7. Li, L.; Wang, L.-L.; Johnson, D.; Zhang, Z.; Sanchez, S.; Kang, J.; Nuzzo, R. G.; Wang, Q.; Frenkel, A. I.; Li, J.; *et al*. Non-Crystalline-to-Crystalline Transformations in Pt Nanoparticles. *J. Am. Chem. Soc.* **2013**, *135*, 13062–13072.
8. Yevick, A.; Frenkel, A. I. Effects of Surface Disorder on EXAFS Modeling of Metallic Clusters. *Phys. Rev. B* **2010**, *81*, 115451.
9. Stern, E. A. In *X-Ray Absorption: Principles, Applications, Techniques of EXAFS, SEXAFS, and XANES*; Koningsberger, D. C., Ed.; John Wiley and Sons: New York, NY, 1988.
10. Mustre de Leon, J.; Rehr, J. J.; Zabinsky, S. I.; Albers, R. C. Ab Initio Curved-Wave X-Ray-Absorption Fine Structure. *Phys. Rev. B* **1991**, *44*, 4146–4156.
11. Bunker, G. Application of the Ratio Method of EXAFS Analysis to Disordered Systems. *Nucl. Instrum. Methods* **1983**, *207*, 437–444.
12. Garcia-Martinez, J. C.; Scott, R. W. J.; Crooks, R. M. Extraction of Monodisperse Palladium Nanoparticles from Dendrimer Templates. *J. Am. Chem. Soc.* **2003**, *125*, 11190–11191.
13. Garcia-Martinez, J. C.; Crooks, R. M. Extraction of Au Nanoparticles Having Narrow Size Distributions from within Dendrimer Templates. *J. Am. Chem. Soc.* **2004**, *126*, 16170–16178.
14. Yancey, D. F.; Zhang, L.; Crooks, R. M.; Henkelman, G. Au@Pt Dendrimer Encapsulated Nanoparticles as Model Electrocatalysts for Comparison of Experiment and Theory. *Chem. Sci.* **2012**, *3*, 1033–1040.
15. Yancey, D. F.; Chill, S. T.; Zhang, L.; Frenkel, A. I.; Henkelman, G.; Crooks, R. M. A Theoretical and Experimental Examination of Systematic Ligand-Induced Disorder in Au Dendrimer-Encapsulated Nanoparticles. *Chem. Sci.* **2013**, *4*, 2912–2921.
16. Newville, M. EXAFS Analysis Using *FEFF* and *FEFFIT*. *J. Synchrotron Radiat.* **2001**, *8*, 96–100.
17. Ravel, B.; Newville, M. *ATHENA*, *ARTEMIS*, *HEPHAESTUS*: Data Analysis for X-Ray Absorption Spectroscopy Using *IFEFFIT*. *J. Synchrotron Radiat.* **2005**, *12*, 537–541.
18. Kresse, G.; Furthmüller, J. Efficiency of Ab-Initio Total Energy Calculations for Metals and Semiconductors Using a Plane-Wave Basis Set. *Comput. Mater. Sci.* **1996**, *6*, 15–50.
19. Perdew, J. P.; Ruzsinszky, A.; Csonka, G. I.; Vydrov, O. A.; Scuseria, G. E.; Constantin, L. A.; Zhou, X.; Burke, K. Restoring the Density-Gradient Expansion for Exchange in Solids and Surfaces. *Phys. Rev. Lett.* **2008**, *100*, 136406.
20. Perdew, J. P.; Burke, K.; Ernzerhof, M. Generalized Gradient Approximation Made Simple. *Phys. Rev. Lett.* **1996**, *77*, 3865–3868.
21. Blöchl, P. E. Projector Augmented-Wave Method. *Phys. Rev. B* **1994**, *50*, 17953.
22. Kresse, G.; Joubert, D. From Ultrasoft Pseudopotentials to the Projector Augmented Wave Method. *Phys. Rev. B* **1999**, *59*, 1758.
23. Roscioni, O. M.; Zonias, N.; Price, S. W. T.; Russell, A. E.; Comaschi, T.; Skylaris, C.-K. Computational Prediction of L3 EXAFS Spectra of Gold Nanoparticles from Classical Molecular Dynamics Simulations. *Phys. Rev. B* **2011**, *83*, 115409.